# ECHO-ENABLED HARMONIC GENERATION*

G. Stupakov, SLAC National Accelerator Laboratory, Menlo Park, CA, USA

*Abstract*

A recently proposed concept of the Echo-Enabled Harmonic Generation (EEHG) FEL uses two laser modulators in combination with two dispersion sections to generate a high-harmonic density modulation in a relativistic beam. This seeding technique holds promise of a one-stage soft x-ray FEL that radiates not only transversely but also longitudinally coherent pulses. Currently, an experimental verification of the concept is being conducted at the SLAC National Accelerator Laboratory aimed at the demonstration of the EEHG.

## INTRODUCTION

There has been continually growing interest in generating coherent and powerful short-wavelength radiation using the free electron laser (FEL) scheme, as reflected by the many proposals and funded projects worldwide [1]. In the nanometer and sub-nanometer wavelengths, the two leading candidates are self-amplified spontaneous emission (SASE) configuration [2, 3] and the high gain harmonic generation (HGHG) scheme [4, 5]. Since the SASE FEL starts from the electron beam shot noise, its output typically has limited temporal coherence and relatively large shot-to-shot fluctuations in both the power and the spectrum. An alternative to the SASE configuration is the HGHG scheme that allows generation of temporally coherent radiation by using up-frequency conversion of a high-power seeding signal.

In the standard HGHG scheme [5], the electron beam is first energy modulated with a seed laser in the undulator (modulator) and then sent through a dispersion region which converts the energy modulation into a density modulation. The density modulated beam is then sent through the second undulator (radiator) tuned to a harmonic of the seed laser. The up-frequency conversion efficiency for this classic HGHG scheme is relatively low: generation of $m$th harmonic of the seed laser requires the energy modulation amplitude approximately equal to $m$ times the slice energy spread of the beam. Because a considerable increase of the slice energy spread would significantly degrade the lasing process in the radiator, the harmonic numbers $m$ used in the standard HGHG scheme are typically no larger than 6. In order to generate coherent soft x-rays with a wavelength in the range of few nanometers using an ultra-violet (UV) seeding laser with the wavelength $\sim 200$ nm, multiple stages of the HGHG FEL are to be used [6].

Recently a new method for generation of high harmonics using the beam echo effect was proposed [7]. The idea of the echo seeding is based on the echo effect in accelerators which was proposed [8, 9] and experimentally studied in hadron accelerator in the range of frequencies 10-100 MHz [10–12] in the past. The echo scheme has a remarkable up-frequency conversion efficiency and allows for generation of high harmonics with a relatively small energy modulation.

## HGHG AND EEHG

In the HGHG approach [4, 5], the beam passes through an undulator-modulator and a dispersive element (chicane). A laser pulse in tune with the frequency of the beam radiation in the undulator and synchronized with the beam, modulates the beam energy with the amplitude $\Delta E$ and the laser wavelength $\lambda_L$. After passage through the chicane with dispersive strength $R_{56}$, the beam gets modulated in density with period $\lambda_L$. This modulation carries various harmonics with the wavelengths $\lambda_L/m$, where $m$ is an integer number. The modulation strength at harmonic $m$ is characterized by the bunching factor $b_m$. Assuming a Gaussian energy distribution of the beam with the rms spread $\sigma_E$, a simple expression can be obtained for $b_m$ [5]. It follows from that expression that the optimal value of the dispersion approximately satisfies $R_{56}\Delta E/E_0 \approx \lambda_L/4$ (assuming $\Delta E \gg \sigma_E$), where $E_0$ is the beam energy. With this optimized dispersion strength, in the limit of large $m$, the absolute value of the bunching factor is

$$|b_m| \approx \frac{0.68}{m^{1/3}} e^{-\frac{m^2}{2A^2}}, \qquad (1)$$

where $A = \Delta E/\sigma_E$.

As follows from this formula in order to obtain large values of $m$, it is required that $A \gtrsim m$. However, very large $A$ would increase the slice energy spread in the beam and result in the degradation of the lasing process in the radiator.

The layout of the EEHG scheme is shown in Fig. 1. The EEHG consists of two modulators and two dispersion sections. The system is followed by a radiator undulator (not shown in Fig. 1). Similar to the HGHG scheme, a laser pulse is used to modulate the beam energy in the first undulator, and then the beam passes through the first chicane. After that a second laser pulse modulates the beam energy in the second undulator and the beam passes through the second chicane. The laser frequencies for the first and the

* Work supported by the U.S. Department of Energy under contract DE-AC02-76SF00515.

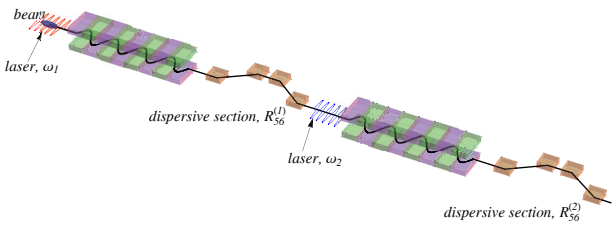


Figure 1: Schematic of the EEHG. The beam energy is modulated in the first undulator (modulator 1) tuned at frequency $\omega_1$ due to the interaction with the first laser beam. After passing through the first dispersion section with $R_{56}^{(1)}$, the beam energy is then modulated in the second undulator (modulator 2), tuned to frequency $\omega_2$, due to the interaction with the second laser beam. The beam then passes through the second dispersion section $R_{56}^{(2)}$.

second modulators, $\omega_1$ and $\omega_2$, in general case are different, but they can also be equal.

Calculations show [7] that at the exit from the second chicane the beam is modulated in the longitudinal direction with the combination of frequencies $\omega_1$ and $\omega_2$. More precisely, the modulations have wavenumbers $k_{n,m}$,

$$ck_{n,m} = n\omega_1 + m\omega_2\,, \tag{2}$$

where $n$ and $m$ are integer numbers. Note that $n$ and $m$ can be either positive or negative, with a negative $k_{n,m}$ meaning a modulation with wavelength $2\pi/|k_{n,m}|$. Using the notation $b_{n,m}$ for the corresponding bunching factor, one finds [13]

$$b_{n,m} = \left|e^{-\frac{1}{2}(nB_1+(Km+n)B_2)^2} J_m\left(-(Km+n)A_2B_2\right)\right. \\ \left. J_n\left(-A_1\left(nB_1+(Km+n)B_2\right)\right)\right|\,, \tag{3}$$

where $A_1 = \Delta E_1/\sigma_E$, $B_1 = R_{56}^{(1)}k_1\sigma_E/E_0$, $A_2 = \Delta E_2/\sigma_E$, $B_2 = R_{56}^{(2)}k_1\sigma_E/E_0$, $\Delta E_1$ and $\Delta E_2$ are the amplitudes of the energy modulation in the first and second modulators, respectively, $R_{56}^{(1)}$ and $R_{56}^{(2)}$ are the $R_{56}$ parameters for the first and second chicanes, $k_1 = \omega_1/c$, $K = \omega_2/\omega_1$, and $J_n$ is the Bessel function of order $n$.

Having four dimensionless parameters $A_1$, $A_2$, $B_1$, and $B_2$ in the problem allows for a much better optimization of the absolute value of the bunching factor $b_{n,m}$ for given $n$, $m$, and the ratio $K$ of the frequencies. Analysis shows that the bunching factor attains its maximum when $n = \pm 1$ and decreases as the absolute value of $n$ increases. Limiting consideration by the case $n = -1$ and $m > 0$ only, one finds

$$b_{-1,m} = \left|J_m\left((Km-1)A_2B_2\right)\right. \\ \left. J_1\left(A_1\left(B_1-(Km-1)B_2\right)\right)e^{-\frac{1}{2}(B_1-(Km-1)B_2)^2}\right|\,. \tag{4}$$

For a given amplitudes $A_1$ and $A_2$ and the number $m$ one can try to choose the dispersion strengths $B_1$ and $B_2$ in such a way that they maximize the value of $b_{-1,m}$. Such maximization was carried out in Ref. [13]. For $m > 4$, the optimal value of $B_2$ is given by

$$B_2 = \frac{m + 0.81m^{1/3}}{(Km-1)A_2}\,. \tag{5}$$

After $B_2$ is found, the optimal value of $B_1$ is computed from

$$B_1 = (Km-1)B_2 + \xi(A_1)\,, \tag{6}$$

where the function $\xi(A_1)$ should be determined from the equation $A_1\left[J_0(A_1\xi) - J_2(A_1\xi)\right] = 2\xi J_1(A_1\xi)$. When both conditions (5) and (6) are satisfied, it turns out that the bunching factor does not depend on $A_2$ and depends only on $A_1$. This dependence is given by $b_{-1,m} \approx F(A_1)/m^{1/3}$, where $F$ is a monotonically increasing function of it argument approaching the value 0.39 in the limit of large values of $A_1$. In this limit the maximal bunching factor becomes (assuming $m > 4$)

$$b_{-1,m} \approx \frac{0.39}{m^{1/3}}\,. \tag{7}$$

Comparing (7) with (1) we see the main advantage of the echo scheme: it allows one to achieve a high modulation at a large harmonic without excessive increase of the modulation amplitudes $A_1$ and $A_2$.

## BEAM ECHO PHASE SPACE

As follows from Eqs. (5) and (6), in the limit of large values of $m$, and assuming $A_1, A_2 \sim 1$,

$$B_2 \approx \frac{1}{KA_2}\,, \qquad B_1 \approx \frac{m}{A_2}\,, \tag{8}$$

which means that the strength of the first chicane becomes large (note that for the harmonic generation in the HGHG discussed above, the optimal value of $R_{56}$ in our units is given by $B \approx \pi/2A$). The large value of $R_{56}^{(1)}$ results in dramatic changes of the longitudinal phase space of the beam. The phase space and the energy distribution function after the first chicane for $B_1 = 12.1$ and $A_1 = 1$ are shown in Fig. 2. The complicated structure of the phase space results from the fact that, due to the large slippage in the first chicane, particles with different energies located initially at various coordinates over the interval $\Delta z \sim R_{56}^{(1)}\Delta E_1/E_0 \gg \lambda_L$ around some value $z$ end up at the same position $z$ after passing the chicane. Correspondingly, the energy distribution function becomes highly modulated in energy, as is shown in Fig. 2. Note also that, if projected onto the $z$ axis, the distribution function in Fig. 2 does not show any density or current modulation.

A subsequent modulation of the beam energy in the second undulator and the passage through the second chicane result in the phase space shown in Fig. 3, for $A_2 = 1$ and $B_2 = 1.3$. The stripes in the phase space of Fig. 2 are

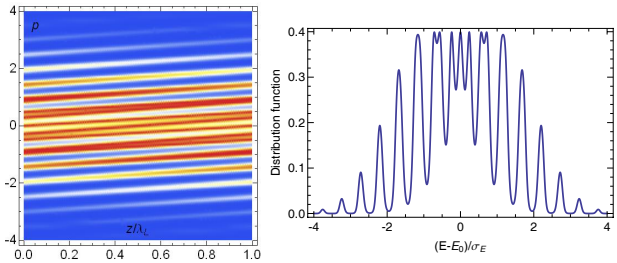


Figure 2: Longitudinal phase space of the beam after passage through the first chicane (left panel) and the corresponding energy distribution of the beam (right panel). The vertical axis on the left panel shows the dimensionless deviation of the energy $p = (E - E_0)/\sigma_E$, and the horizontal axis is the longitudinal coordinate $z$ normalized by the laser wavelength $\lambda_L$. Only one period of the modulation is shown. The energy distribution is calculated for position $z/\lambda_L = 0.5$.

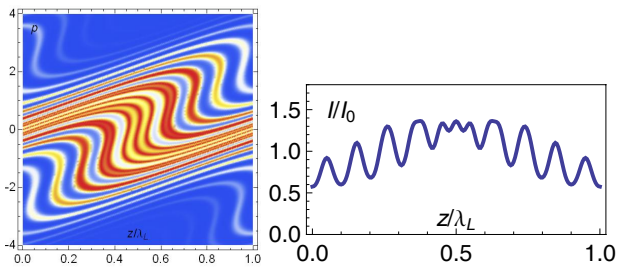


Figure 3: Longitudinal phase space of the beam after passing through the second chicane (left panel) and the corresponding current distribution of the beam (right panel). The current distribution is shown for one period of modulation $\lambda_L$.

now stretched and rotated by ninety degrees in their middle parts in such a way that their projection onto the $z$ axis generates modulation of the beam density and the current. The corresponding current modulation is shown in the right panel of Fig. 3: the maximal harmonic bunching factor in this modulation corresponds to the harmonic $m = 10$ with the bunching factor $b_{10} \approx 0.08$.

## EEHG APPLICATIONS

To illustrate a possible application of the EEHG in a system with realistic parameters, we take the nominal parameters of the Fermi@Elettra FEL project [14] and show below how the 24th harmonic of the seed laser can be generated with a relatively small energy modulation using the EEHG scheme. The electron beam energy of the Fermi@Elettra FEL is 1.2 GeV and the slice energy spread is 150 keV. We assume the wavelength of the seed laser 240 nm with the frequency of the first and the second modulators equal, $\omega_1 = \omega_2$. The energy modulation amplitudes in modulator 1 and modulator 2 are chosen to be $A_1 = 3$ and $A_2 = 1$, respectively. Note that the energy modulation amplitude in our example is much smaller than the nominal value of the modulation amplitude in the Fermi@Elettra project. The optimized dispersion strengths obtained from Eqs. (5) and (6) that maximize the bunching factor for the 24th harmonic are found to be $B_1 = 26.83$ and $B_2 = 1.14$, corresponding to $R_{56}^{(1)} = 8.20$ mm and $R_{56}^{(2)} = 0.35$ mm, respectively. The maximal displacement of the electrons in the longitudinal direction after passing through the first dispersion section is about $\Delta z \approx 13\lambda_L$ that is small compared to the overall bunch length.

## ISSUES AFFECTING EEHG

There are several practical considerations that were neglected in the simple one-dimensional model of EEHG described in the previous sections. Among the most important of them are the incoherent synchrotron radiation (ISR) and the coherent synchrotron radiation (CSR) of the beam in dipole magnets of the dispersive elements of the system.

Due to the relatively large dispersion strength in the first chicane ISR may affect the performance of the echo seeding. The energy diffusion in the process of radiation caused by the quantum fluctuations can lead to a deterioration of the EEHG. If the rms energy spread caused by this diffusion exceeds the spacing of two adjacent energy bands (see Fig. 2), the bands overlap and smear out the fine structures of the longitudinal phase space thus degrading the EEHG modulation.

One can easily estimate the energy diffusion by calculating the energy spread $\Delta\sigma_E$ due to a passage of a charged particle through a bend of length $L$ and bending radius $\rho$ [15]:

$$\Delta\sigma_E^2\big|_{ISR} = \frac{55e^2\hbar c}{24\sqrt{3}}\frac{L}{\rho^3}\gamma^7\,, \qquad (9)$$

where $\gamma$ is the relativistic factor and $\hbar$ is the reduced Planck constant. A quick estimate shows that for the beam energy $\sim 1$ GeV, the bending radius of a few meters and the length of order of a meter, the energy spread due to the ISR can be of the order of few kiloelectronvolts, or even as small as a fraction of keV, and is smaller than the energy spread for the cases considered in the previous section. However, a steep dependence of $\Delta\sigma_E$ on the beam energy imposes additional constrains on the design of chicane magnets for a high-energy EEHG device.

If the density modulation of the beam occurs inside the magnets of the chicane, it would cause coherent synchrotron radiation and a concomitant energy modulation inside the dispersive section, which may result both in the emittance growth of the beam and the distortion of the phase space structures required for the echo modulation. Fortunately, there is a strong suppression effect due to a smearing of such modulation caused by nonzero values of the parameters $R_{51}$ and $R_{52}$ inside the chicanes. Typically, the dominant smearing is due to $R_{51}$, and the suppression

factor for a Gaussian transverse beam profile is [16, 17]

$$e^{-k_{\rm mod}^2 R_{51}^2 \sigma_x^2/2}\,, \qquad (10)$$

where $k_{\rm mod}$ is the wave number of the modulation and $\sigma_x$ is the transverse rms size of the bunch in the magnet. For representative numbers $\sigma_x \sim 40$ $\mu$m, $R_{51} \approx 0.01$, one finds that modulation with the wavelengths less then $\sim 1$ $\mu$m will be extinguished and hence the CSR will be suppressed.

One can use Eq. (10) to establish an important tolerance on the quality of the magnetic field of the chicanes. An ideal chicane has $R_{51} = 0$ at the exit. According to (10) a leaking nonzero value of $R_{51}$ from the chicanes can smear out the microbunching generated in the system. This leakage should be carefully controlled and minimized at the level which does not deteriorate the EEGH.

There are also other requirements on the system that should be satisfied in order not to destroy a small-scale echo microbunching. They are discussed in more detail in Refs. [13, 18, 19].

## PERFORMANCE OF THE EEHG FEL

To illustrate a possible performance of the EEHG FEL [13] we again use parameters of the Fermi@Elettra FEL project for the case of 10 nm radiation wavelength.

The energy modulation and the dispersion strengths were chosen to be the same as described above to maximize the bunching factor for the 24th harmonic. The first modulator was chosen to be 135 cm long with the undulator period length of 15 cm. The input laser had a waist of 310 microns and the peak power of 64 MW. The corresponding energy modulation amplitude was $A_1 = 3$. The second modulator was 45 cm long and had just 3 undulator periods. The second laser parameters were the same and the corresponding normalized energy modulation amplitude was $A_2 = 1$.

The simulation was performed with the upgraded code Genesis [20, 21]. The radiator undulator had a period of 5 cm and was divided into 6 sections of 2.5 m separated by 0.5 m drift for focusing and beam diagnostics.

During the simulation, the dispersion strength and power of the seed laser were finely tuned to maximize the bunching factor for the 24th harmonic at the entrance to the radiator. The evolution of the bunching factor and radiation power are shown in Fig. 4. The significant enhancement of the performance using the EEHG scheme is clearly seen in Fig. 4b where the peak power of the 24th harmonic radiation exceeds 1.6 GW and it saturates after 5 undulator sections (the total magnet length is 12.5 m). The large bunching factor at the entrance to the radiator offered by the EEHG scheme is responsible for the initial steep quadratic growth of the power. The high peak power and short saturation length should be attributed to the initial large bunching factor and the small energy modulation in the modulators. Indeed, the local energy spread at the entrance to the radiator is only about 2.45 times larger than the initial local energy spread.

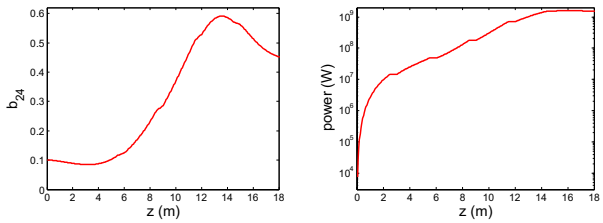


Figure 4: (a) Bunching factor vs radiator distance for the 10 nm radiation; (b) Peak power vs radiator distance for the 10 nm radiation.

With the same beam and laser parameters, the performance of an EEHG FEL was also simulated at the 48th harmonic, with the radiation wavelength of 5 nm. The results of that simulation can be found in Ref. [13].

As a further development of the EEHG scheme, in reference [22], it was shown that ultrashort pulses of x-ray radiation can be generated by adding a few more elements to the original scheme of the echo modulation. In a recent paper [24] an echo-based scheme to generate two attosecond x-ray pulses with different carrier frequencies and variable delay has been proposed for x-ray stimulated Raman spectroscopy.

## PROOF-OF-PRINCIPLE EXPERIMENT AT SLAC

A proof-of-principe experiment to demonstrate EEHG is currently being conducted at SLAC National Accelerator Laboratory [25, 26], Fig. 5. The existing NLCTA facil-

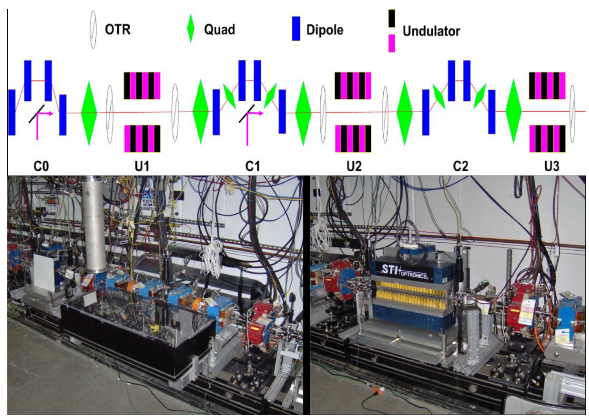


Figure 5: Layout of the echo-seeding experiment (top) and photographs of the chicane C1 (bottom left) and the undulator U2 (bottom right).

ity which houses an S-band photocathode electron gun and an X-band accelerator is used for the experiment. The parameters of the experiment are summarized in Table 1. In the experiment, the beam is first energy modulated in the first modulator U1 using a Ti:Sapphire laser with the wavelength 795 nm and then sent through the chicane C1 with

Table 1: Main Beam and Laser Parameters

| | |
|---|---|
| Electron beam energy | 120 MeV |
| Normalized emittance | $< 8\,\mu$m |
| Slice energy spread | $< 10$ keV |
| First laser wavelength | 795 nm |
| Second laser wavelength | 1590 nm |

a strong dispersion. A second laser from the optical parametric amplifier (1590 nm) is used to modulate the beam energy in the second modulator U2. The experiment aims at generating the 5th and 7th harmonics of the second laser via the echo mechanism. The beam modulation will be measured with the help of a third undulator U3 which can be tuned either to the 5th (318 nm) or to the 7th (227 nm) harmonic of the second laser.

The commissioning run of the experiment has started in April 2010. One of the preliminary results from this run is shown in Fig. 6. The images are recorded with a UV-

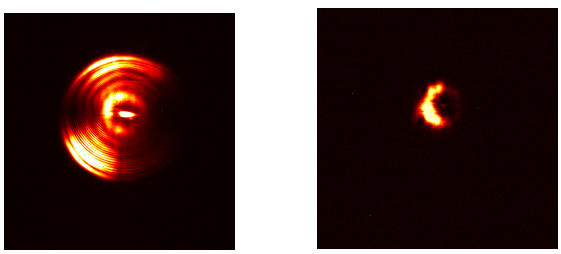

Figure 6: Radiation intensity on the OTR screen downsteam of the last undulator with (right) and (withouth) the bandpass filter.

sensitive CCD at the exit after U3 undulator tuned to 318 nm when both lasers interact with the beam. To confirm that there is radiation at the 4th harmonic of the 1590 nm laser, a 10 nm bandpass filter centered at 395 nm was put in front of the CCD camera and the result is shown in the right plot of Fig. 6.

More details of the SLAC echo experiment can be found in the papers presented at this conference [25, 26].

## CONCLUSIONS

The proposed approach of the echo-enhanced harmonic generation provides a new promising way to introduce a controlled density modulation in an electron beam at a high harmonic of the laser frequency. It opens new possibilities in generation of coherent soft x-rays from free electron lasers, with an option that includes extremely short, attosend-duration pulses.

## ACKNOWLEDGEMENTS

The author would like to thank his collaborator Dao Xiang, who made crucial contributions to many subjects covered in this report, and Zhirong Huang for many useful discussions.

This work was supported by the U.S. Department of Energy contract DE–AC02–76SF00515.

## REFERENCES

[1] C. Pellegrini. In *Proc. EPAC, Edinburgh, 2006*, p. 3636, 2006.

[2] A. Kondratenko and E. Saldin. *Particle Accelerators*, **10**, p. 207, 1980.

[3] R. Bonifacio, C. Pellegrini, and L. M. Narducci. *Optics Communications*, **50**, p. 373, 1984.

[4] R. Bonifacio *et al.*, *Nucl. Instrum. Meth.*, **A296**, p. 787, 1991.

[5] L. H. Yu. *Phys. Rev. A*, **44**, p. 5178, 1991.

[6] J. Wu and L. H. Yu. *Nucl. Instrum. Meth.*, **A475**, p. 104, 2001.

[7] G. Stupakov. *Phys. Rev. Lett.*, **102**, p. 074801, 2009.

[8] G. Stupakov. Preprint SSCL-579, SSCL, 1992.

[9] G. Stupakov and S. Kauffmann. Preprint SSCL-587, SSCL, 1992.

[10] L. K. Spentzouris, J.-F. Ostiguy, and P. L. Colestock. *Phys. Rev. Lett.*, **76**, p. 620, 1995.

[11] O. Brüning *et al.*, in PAC 1997, p. 1816, 1997.

[12] E. Shaposhnikova. Report CERN SL/note 95-125 (RF), CERN, 1995.

[13] D. Xiang and G. Stupakov. *PRST-AB*, **12**, p. 030702, 2009.

[14] C. J. Bocchetta *et al.*, Conceptual design report for the FERMI@ELETTRA. Report ST/F-TN-07/12, ELETTRA, 2007.

[15] A. Chao and M. Tigner. *Handbook of Accelerator Physics and Engineering*. 3d ed., 2006.

[16] S. Heifets, G. Stupakov, and S. Krinsky. *PRST-AB*, **5**, p. 064401, 2002.

[17] Z. Huang and K.-J. Kim. *PRST-AB*, **5**, p. 074401, 2002.

[18] Z. Huang *et al.*, Preprint SLAC-PUB-13547, SLAC, 2009.

[19] D. Xiang and G. Stupakov. Preprint SLAC-PUB-13644, SLAC, 2009.

[20] S. Reiche. *Nucl. Instrum. Meth.*, **A429**, 243, 1999.

[21] S. Reiche, P. Musumeci, and K. Goldammer. In *Proceedings of the 2007 PAC*. IEEE, 2007.

[22] D. Xiang, Z. Huang, and G. Stupakov. *PRST-AB*, **12**, p. 060701, 2009.

[23] D. Xiang *et al.*, In *Proc. of the 2009 FEL Conf.*, Liverpool, UK, 2009.

[24] A. Zholents and G. Penn. *Nucl. Instrum. Meth.*, **A612**, 254, 2010.

[25] D. Xiang *et al.*, Paper TUPE072, these proceedings.

[26] C. Hast *et al.*, Paper TUPE069, these proceedings.